Materials and Design 162 (2019) 263–270

Contents lists available at ScienceDirect

Materials and Design

journal homepage: www.elsevier.com/locate/matdes

Optimization of extrusion based ceramic 3D printing process for complex bony designs

Uday Kiran Roopavath [a,c], Sara Malferrari [a], Annemieke Van Haver [b], Frederik Verstreken [b], Subha Narayan Rath [c], Deepak M. Kalaskar [a,*]

[a] Institute of Musculoskeletal sciences (IOMS), UCL Division of Surgery and Interventional Science, Royal National Orthopaedic Hospital-NHS Trust, HA7 4LP, United Kingdom of Great Britain and Northern Ireland
[b] Monica Hospital, Monica Orthopedic Research (MORE) Institute & University Hospital Antwerp, Belgium
[c] Department of Biomedical Engineering, Indian Institute of Technology Hyderabad, Kandi, Medak-502285, Telangana, India

HIGHLIGHTS

- Extrusion based 3D printing was validated as the accurate and reliable method for hydroxyapatite scaffold manufacturing.
- Infill density and shrinkage of 3D printed hydroxyapatite scaffolds follow a linear relationship.
- It is possible to accurately predict % shrinkage of ceramic green bodies and rescale design files to optimise 3D printing
- Comprehensive modulus of 3D printed scaffolds ranges from 33 - 200 MPa, comparable to human cortical bones (100 to 150 MPa)
- Complex patient specific bone graft is 3D printed accurately from patients own CT scans

GRAPHICAL ABSTRACT

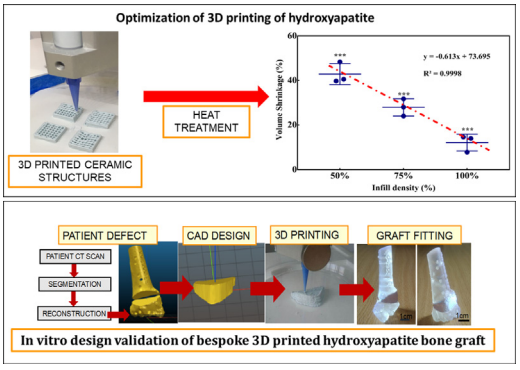

ARTICLE INFO

Article history:
Received 8 August 2018
Received in revised form 25 November 2018
Accepted 26 November 2018
Available online 27 November 2018

Keywords:
3D printing
Hydroxyapatite
Patient specific bone printing
Bone graft
Radial fracture

ABSTRACT

In this study presents materials and design optimization of clinically approved hydroxyapatite (HA) using extrusion based 3D printing process. The effect of various printing parameters including print speed, extrusion pressure, accuracy and infill density to produce defined porous structures is established using various techniques. Particularly Scanning Electron Microscopy, Micro Computed Tomography have been employed to study internal and external accuracy. Mechanical testing was employed to study the effect of porosity on compressive properties of 3D printed structures.

This study shows that, the infill density and shrinkage of 3D printed HA scaffolds post sintering have a linear relationship. Porosity and mechanical strength of 3D printed scaffolds depend on the infill density of the designed CAD file. Tailoring infill density also helps in altering mechanical properties in a predictable manner. Finally, a case study on hydroxyapatite printing of a patient specific bone graft demonstrates the ability of this material and technique to print complex porous structures created on CT-based anatomical bone models and pre-operative 3D planning, providing further promise for custom implant development for complex bony designs.

* Corresponding author.
E-mail address: d.kalaskar@ucl.ac.uk (D.M. Kalaskar).

https://doi.org/10.1016/j.matdes.2018.11.054

1. Introduction

The ability of the bone tissue to repair and remodel on its own to meet mechanical demands of the human body makes it a unique and essential structural composite. Bone is composed of inorganic minerals (calcium phosphates (CaP)) and organic matrix, mostly Collagen Type I. Hydroxyapatite (HA), tricalcium phosphate (TCP) and biphasic calcium phosphates (the mixture of HA and TCP) are very common bioceramic materials used for bone therapy and to replace various bone defects due to their similarity with the inorganic component of the bone. These materials are mainly used in the form of granules, coatings, beads or injectable cement. This limits their usage in small bone defects. Ceramic based scaffolds in cuboidal or cylindrical blocks are also used since they come in pre-determined shapes and sizes, however they need to be shaped during surgery to match bone defects [1,2]. This requires extra time for preparation, increases the surgery time, and the patient exposure. Furthermore, achieving an optimal shape-matching with the patient's defect, remains challenging especially with more complex irregular shapes.

3D printing or additive manufacturing provides the ability to accurately produce complex anatomical shapes and patient specific instruments based on CT/MRI scans. 3D information from a computer model is transformed into a 3D object in a layer by layer manner. Ceramics have been 3D printed using different printing technologies such as Stereolithography (SLA), Digital Light Processing (DLP), Fused Filament Fabrication (FFF) and Direct Ink Writing (DIW) [3–6]. Although SLA, DLP often permits to print with higher resolution compared to extrusion based technologies (such as FFF), they have some drawbacks that make their application into surgery undesirable. For example, HA has successfully been printed with SLA [7], however during this process, HA powder is often mixed with acrylate based photopolymers. If unreacted these monomers lead to in vivo leaks causing damage to cells and nearby tissues [8]. In addition, these technologies often involve several steps before and after printing which delay the manufacturing time [7,9]. Furthermore, the crosslinking is slow and high ink volumes are required as the tank needs to be constantly full, which is associated with high costs for production [10,11]. HA has also been printed with DLP which is faster than SLA as one layer can be crosslinked at the time [11], however, several steps are required pre- and post-printing [12], increasing the manufacturing time. FFF, which is also an extrusion based 3D printing technique permits to print HA at relatively low cost. However, HA needs to be mixed with thermoplastic materials such as Polycaprolactone (PCL) [13] or Polylactic acid (PLA) [14], that increase the degradation time in vivo for bone remodelling. DIW ceramic 3D printing involves preparation of highly viscous ceramic slurry by homogenously mixing the ceramic powder with a polymeric binder. This slurry is extruded using a screw extruder or a compressor in a layer by layer manner to build 3D structures. HA has been successfully printed using DIW methods, however, the ink fabrication often requires several steps and consumables which makes it slow and expensive [15,16].

For ceramic based printing, various material properties are required to be taken into consideration. This includes particle size and their distribution, type and choice of the binder and their composition, viscosity, extrusion pressure [17]. Previous studies [18–20] showed that a mean particle size between 20 and 100 μm and spherical granule morphology produce acceptable results during the 3D printing process. If the particle size is close to the nozzle diameter it can affect the printing parameters such as extrusion pressure and viscosity leading to clogging of the nozzle especially in the case of robocasting or DIW.

3D printing (3DP) methods have several advantages in the clinical field. 3D design modeling gives the surgeon the ability to perform virtual osteotomy resections for precise preoperative planning and designing of patient specific implants prior to surgery. These 3D models can be imported into an advanced image processing visualization software for precise placement of bone grafts. Recent advances in manufacturing and material science has led to the possibility of converting such virtual model or 3D design into reality as surgical guides, physical replica models for intraoperative use and patient specific implants using 3D printing technology [21]. Fabrication of custom designed patient grafts for the reconstruction of bone defects have recently gained importance over their generic counterparts such as allografts and xenografts due to their low cost, availability and desired clinical outcome [22].

Most of the previous studies have used time consuming protocols and focused on printing simple structures such as cubes or cylinders with a resolution of around 1 mm [3,23,24]. It is a widely-accepted fact that 3D printing complex structures like radius or vertebrae is complicated and remains challenging. Also, 3D printing of ceramic materials requires an additional sintering step to remove binder materials, where the material is heat treated beyond 1200 °C [25]. During this process of binder removal, the size of the final product varies to a greater extent from the designed file. Parameters like binder properties, sintering temperature, and porosity affect the size and mechanical properties of the ceramic based printed structures [26–29]. Previous study suggests that 3D printed HA-alginate scaffolds can be stabilized by sintering or by covalent crosslinking of calcium ions [30]. However, the mechanical strength achieved during this process is significant low. Also due to the shrinkage of 3D printed HA scaffolds following sintering process, these scaffolds cannot be used directly as a patient graft, as the obtained size of graft significantly varies from the designed graft.

This study aims to simplify the materials and design process for 3D printing of clinically approved HA so that dimensionally accurate and mechanically stable patient specific complex bony structures can be printed. Materials optimisation was achieved by studying various compositions of HA and hydroxyl propyl methyl cellulose (HPMC) as binder using extrusion based printing process. Design optimisation and effect of sintering on final size and porosity of 3D printed HA structures was analysed using high resolution scanning electron microscopy, micro CT analysis, to predict relation between design files and final process objects. Finally, a clinical case study is presented to validate bone graft printing for a distal radius correction to show that patient specific defects can be 3D printed on demand using extrusion based 3D printing technology from CT-based anatomical data. This study shows real life application of 3D printing technology for pre-surgical planning and patient specific bone graft production from CT scans of patients.

2. Materials and methods

2.1. Preparation of HA ceramic ink

HA powder with a granular size of ~25 μm is obtained from, Ceramisys Ltd., UK, (HA sintered, lot no 1514). Reagent grade Hydroxy propyl methyl cellulose (HPMC) (Sigma Aldrich, UK) is used as a polymeric binder to prepare a ceramic slurry. 4 g of HA powder is mixed with 2 g of 1.5 wt% HPMC solution to obtain a homogenous viscous ceramic ink.

2.2. Computer aided design (CAD) and 3D printing of HA scaffolds

CAD of cuboidal scaffolds (10x10x7 mm) was made with Solidworks (Dassault Sytèmes) and an stl. File is processed with Slic3r (v. 1.2.9 copyright © 2011–2015 Alessandro Ranellucci) for printing. A 3D cuboidal structure with dimensions (10 × 10 × 7 mm) was designed and sliced into three different stl files with 50%, 75% and 100% infill density. Linear infill pattern is employed for all layers, independently from the infill density percentage, as it is the most reliable pattern to create uniform porous structures even for low infill densities and permits a fast and facile fabrication process [31,32]. Extrusion based INKREDIBLE+ (Cellink AB) 3D bioprinter is used for 3D printing the ceramic slurry. The parameters of 3D printing, type of scaffolds and sample codes are shown in Table 1. After 3D printing, the scaffolds were dried at 120 °C in a hot air vacuum oven (Vacutherm, Thermo scientific™). Cuboidal

scaffolds were sintered at 1350 °C at a heating rate of 2 °C/ min with a holding time of 4 h. The scaffolds were then cooled to room temperature at a cooling rate of 10 °C/ min [20,33].

2.3. Scaffold characterization

2.3.1. Quantification of the external volume

Dimensions of the fabricated scaffolds (n = 3) immediately after 3D printing and after sintering was measured manually using a Vernier callipers. The measured external dimensions of the scaffolds after sintering are considered as total experimental external volume and were used for further analysis.

2.3.2. Mechanical testing

Measurement of the compressive strength of the scaffolds was carried out using a Zwick Roell zwickiLine Z0.5 low-force mechanical tester with a crosshead speed of 5 mm/min. The samples were placed onto a metal platform and the load was applied up until around 2 mm in standard travel from the point of contact of the crosshead and scaffold surface. This range was chosen to prevent measurement error from the dense compaction of the powders. A total of n = 4 was chosen for each of the 3 conditions with different infill densities.

2.3.3. Scanning Electron microscopy (SEM) analysis

The surface morphological properties of all the three types of scaffolds with different infill densities are characterized using a scanning electron microscopy (SEM, JASP 5500; UK). All the scaffolds types were sputter coated with platinum for 3 min in order to obtain a coating of ~10 nm and images were obtained with an operating voltage of 5 KV at different resolutions.

2.3.4. X-ray microcomputed tomography (micro-CT)

A high-resolution X-ray microcomputed tomography (micro-CT) imaging system (Skyscan 1172, Bruker, Kontich, Belgium) was used to take a non-destructive qualitative image of the 3D microstructure of the scaffolds and to carry out a quantitative 3D analysis of the porosity, volume fraction and degree of anisotropy in the selected volume of interest (VOI) for all the samples with different infill densities (50%, 75% and 100%) before and after sintering the scaffolds were fixed onto a metal stub and placed within the x-ray chamber. They were subsequently scanned with a voxel resolution of 9.97 μm using an Aluminium filter (0.5 mm) and an exposure time of 1169 ms whilst being rotated 360°. The scan data was then reconstructed (total of 400 slices) with NRecon software (Bruker) to smooth the slices, correct beam hardening and reduce ring artefacts. The reconstructed data was then analysed using CT-scan software (Bruker, USA). A volume of interest reference point was selected in the middle of the scaffold and then expanded to 150 slices above and 150 below to select the section for 3D analysis. To reduce image noise a Gaussian filter was applied using the same parameters for each of the other scans. The data was then segmented to distinguish the scaffold boundaries from the surrounding space based on the grey scale value and this was consistently repeated for all scaffolds. To measure the orientation of internal structures with in the volume of cuboidal scaffolds, degree of anisotropy (DA) was measured in the VOI for all infill densities. DA is measured as $DA = \frac{1-long\ axis\ eigen\ value}{short\ axis\ eigen\ value}$ obtained with in the VOI.

2.3.5. Validation of the ink formulation and 3D printing process with a clinical case

The optimization of the ink formulation and 3D printing process was validated with a clinical case of the distal radius fracture. Briefly, CT scan of distal radius malunion was reconstructed and the required clinical defect and graft were reconstructed and designed using CT imaging (Somatom Sensation 64 CT scanner: slice thickness, 0.6 mm; slice increment, 0.6 mm; image matrix, 512 × 512 pixels; pixel size, 0.269 mm; Siemens Healthcare, Erlangen, Germany) from the elbow to the carpometacarpal joints was performed. The DICOM files were imported into medical image processing software (Mimics and 3-Matic; Materialise N.V., Leuven, Belgium) to segment the CT images and generate 3-dimensional virtual models of both forearm bones. Consequently, a virtual osteotomy was performed to produce a precise correction of angular and rotational malalignment of the radius. Since the models were fully anonymized; no ethical approval is necessary. The obtained 3D model of the patient defect is 3D printed with a clear resin (Clear resin V2) using high resolution SLA printer Formlabs 2 (Formlabs). The obtained CAD of the patient defect graft is scaled up to compensate for shrinkage post sintering process, and 3D printed using HA ink (60% infill density). After sintering, the graft was glued inside the defect and a CT scan of the entire construct was taken for quality control. The graft was reconstructed using ScanIP 2018.03 (Simpleware Ltd) and its volume was obtained using the "volume measurement function" of ScanIP CAD module and compared to the original designed graft. The distance mapping between the printed graft and the bone defect was assessed using the "polydata distance filter" of Paraview (Kitware Inc.)

2.4. Statistical analysis

Results are presented as mean ± standard deviation. Statistical analysis was performed for all the results using GraphPad Prism software (GraphPad Software, San Diego, CA, USA). A one-way analysis of variance (ANOVA) followed by Bonferroni's post hoc test was used to determine the level of statistical significance. P values < 0.05 were considered as statistically significant.

3. Results & discussions

3.1. Validation of printing accuracy for printed HA structure

Printing accuracy of HA based structure was tested by printing standard cuboidal structures of known dimensions and infill densities. Viscosity of the prepared slurry was optimised by varying powder to binder ratio and extruding final composition through a syringe with 22G nozzle. Optimised viscosity of HA-ink is required to build 3D layer by layer structures which hold its shape during printing. Very low viscosities do not facilitate 3D printing of layers, whereas very high viscosities require high extrusion pressures and often lead to clogging of the nozzle which in turn affects the accuracy of 3D printed structures. Print speed was kept constant at 10 mm/s, increasing or decreasing the print speed further affects the accuracy of the 3D printed structures.

Table 1
Table showing the parameters of 3D printing and dimensions of the average external volume of the scaffolds after 3D printing and post sintering process for various infill densities. * indicates the ±mean standard deviation.

Sample code	Infill density	Extrusion pressure	Print speed	External volume of design file	Average external volume after 3D printing	Average external volume after sintering	% Shrinkage in external volume after sintering
50% infill	50%	100–200 KPa	10 mm/s	700 mm^3	709 ± 4.84 mm^3	490 ± 15.93 mm^3	42 ± 4.72%*
75% infill	75%	100–200 KPa	10 mm/s	700 mm^3	722 ± 12.60 mm^3	547 ± 16.56 mm^3	28 ± 3.86%*
100% infill	100%	100–200 KPa	10 mm/s	700 mm^3	786 ± 18.61 mm^3	628 ± 18.14 mm^3	12 ± 3.75%*

Polymeric binder is used to provide adequate viscosity to HA ink formulation during printing process. It also helps to bind individual ceramic particles together during printing process so that printed structure layers remain stable and can bear weight of subsequent deposited layers in three dimensions. Polymer binder is relatively inert material and does not react with HA or undergo any chemical reaction. As temperature is gradually increased during sintering process, the binder is burnt out at 350 °C leaving only HA to sinter gradually until temperate reaches 1350 °C, as described in materials and methods section. During sintering at 1350 °C, HA particles bind together and provide required mechanical strength to scaffold. FTIR image (supplementary information) shows that there is no chemical reaction between binder residue and HA granules during the process of sintering. All the dominant peaks PO_4^{3-} corresponding to pure hydroxyapatite can be observed in 3D printed samples after sintering. To evaluate accuracy of printing process both external dimension and internal structure (porosity) was evaluated using Vernier calliper, scanning electron microscopy and Micro CT respectively. Fig. 1 shows design file (.stl) and images of corresponding printed structures at 3 different infill densities. Printing accuracy was tested by measuring external volume of printed structure and comparing it with cad design file (as shown in Fig. 2, Table 1). Design file has external volume of 700 mm^3. However after printing, average external experimental volume of printed cubes increases as infill density increases. This is primarily due to increasing amount of material deposited during printing process as infill density increases and spreading of underlying layers due to weight of next layer extruded on top of the previous layer. However, all ceramic scaffolds undergo sintering process to remove binder material and as a result they shrink in their size. This is well known phenomenon which happens due to removal of binder during sintering process [25,34–36]. Fig. 2 and Table 1 show shrinkage of average external volume for all samples after sintering process. The average external volume after sintering is less for 50% and 75% infill when compared to 100% infill density. However, from Fig. 2 it is clear that average external volume after sintering is proportional to infill density, and follows a linear relationship, which can be expressed mathematically by equation.

$y = -0.6138\times + 73.69$ where, y is the percentage volume shrinkage and x is the infill density (%).

This relationship between volume shrinkage and infill density can be used to accurately predict level of shrinkage for 3D printed geometries using HA ink developed in this study. This thus allows us to use this information to scale up geometries during design process, so that accuracy of final print, post-sintering process is maintained. Clinical example of this is presented later in the study.

Accuracy of internal porous structures was evaluated using high resolution scanning electron microscopy (SEM) and MicroCT analysis. Fig. 3(A and B) shows the uniform line thickness in all the scaffold types which is ~200 μm. The layer thickness and resolution of the 3D printing process was observed to be ~200 μm as evident from SEM images. They indicate the decrease in the proximity of lines as the infill density increases. Images in Fig. 3C represent the cross-sectional images obtained from micro CT imaging. They appear to be in close agreement with the SEM images, where presence of porous structure can be seen clearly.

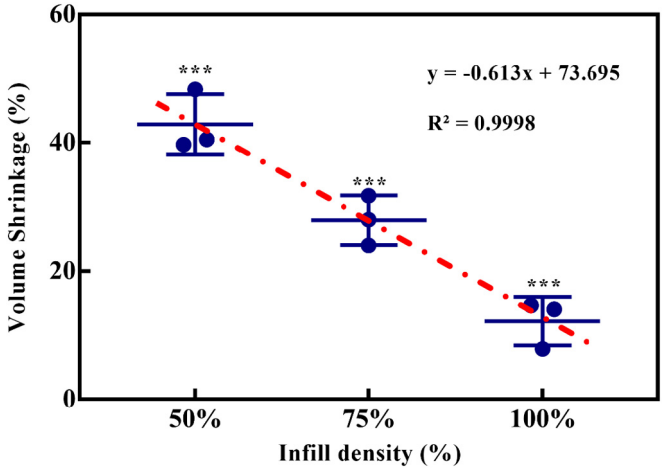

Fig. 2. Graphs showing the percentage shrinkage in external volume of scaffolds at different infill densities after sintering at 1350 °C with respect to their respective computational external volume (*** indicates the statistical significance with $P < 0.001$).

To understand the effect of sintering on the internal porous structure of the scaffolds, quantification using micro CT analysis was undertaken (Fig. 4). The porosity of 50% infill density sample is in a close agreement with design file in terms of fill density, whereas for 75% and 100% infill samples shows values of $33 \pm 4.41\%$ and $5 \pm 1.40\%$ respectively. The assessment of the degree of anisotropy (DA) for all volumes of interest (VOIs) (Table 2) indicates that there is no significant difference in the samples with different infill densities and infill density on its own as a parameter has not contributed to the anisotropy of the 3D printed HA scaffolds.

Various parameters such as print speed, extrusion pressure, viscosity of the ceramic ink etc., [20,26,37–39] play a major role in extrusion based fabrication technique, all these factors contribute to porosity of scaffold before sintering. During the process of sintering, the binder is slowly removed when the temperature reaches ~350 °C. As evident from high magnification SEM images in Fig. 5, polymer used as the binder is found to be attached to individual particles in printed structures and is removed after scaffolds were sintered. After the binder is eliminated from the scaffold matrix, the rise in temperature causes particles to vibrate causing particles to come closer to each other to attain stability [17]. This factor also contributes to change in final porosity (infill density) of the scaffolds. Porosity of $5 \pm 1.40\%$ observed for 100% infill samples is due to the binder removal following the sintering process.

3.2. Mechanical stability of printed HA scaffolds

HA particles size and shape do not seem to change significantly in as printed structures and sintered structure as seen from Fig. 5A

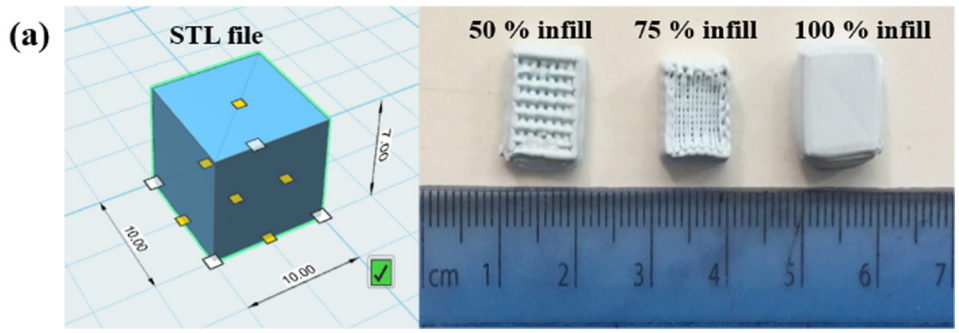

Fig. 1. Images of STL file and 3D printed HA Cube scaffolds at different infill densities sintered at 1350 °C.

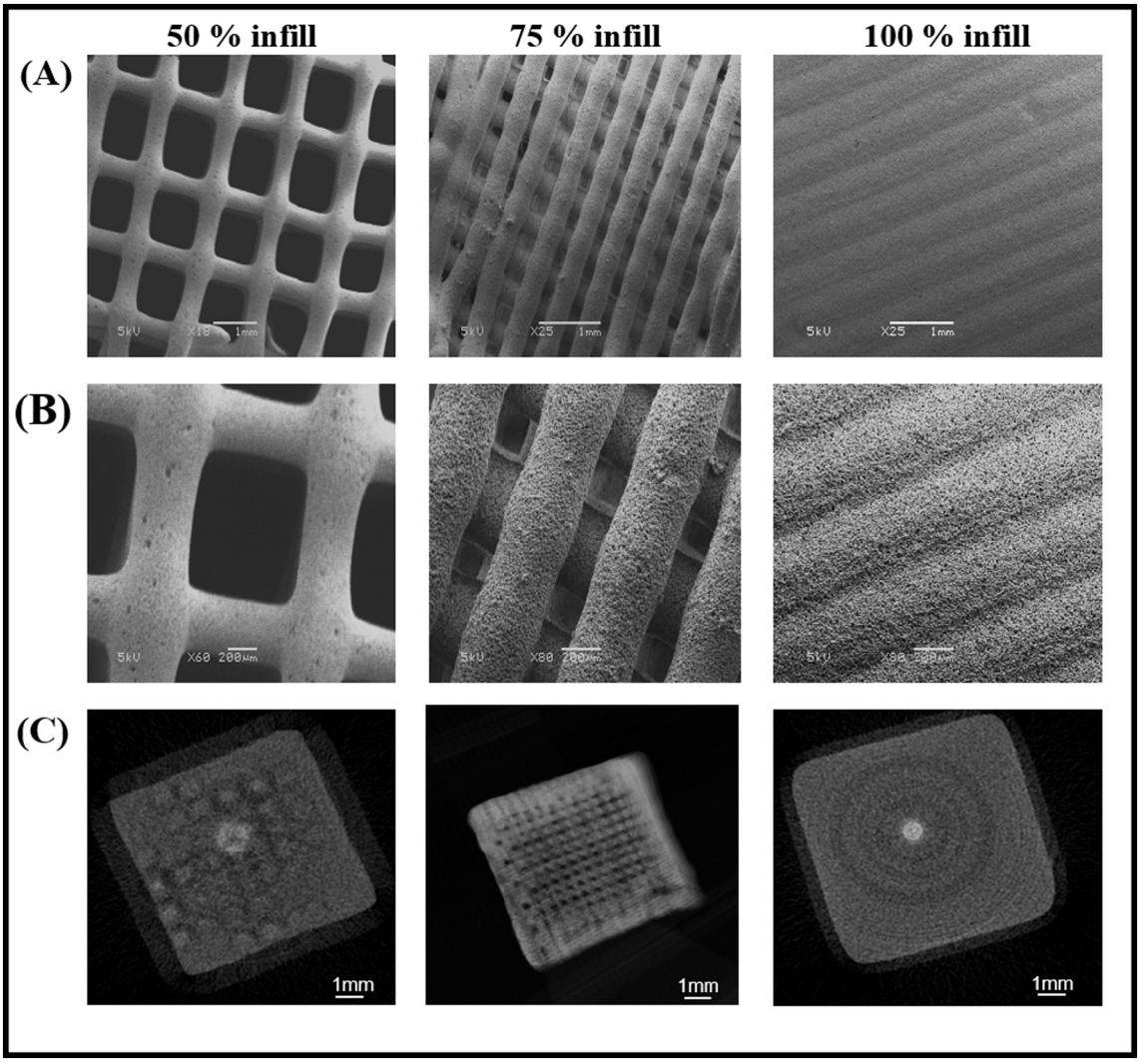

Fig. 3. SEM images of 3D printed CHA scaffolds at different infill densities (A&B) and 3D crossectional Micro-CT Images of 3D printed CHA scaffolds at different infill densities (C). Scale bar for (A) and (C) is 1 mm and for (B) is 200 μm.

and B respectively. Since binder used in this process is water soluble, un-sintered samples are unstable in aqueous solutions [28]. Sintering process which removes binder and help sinter HA particles together via thermal binding improves their mechanical strength.

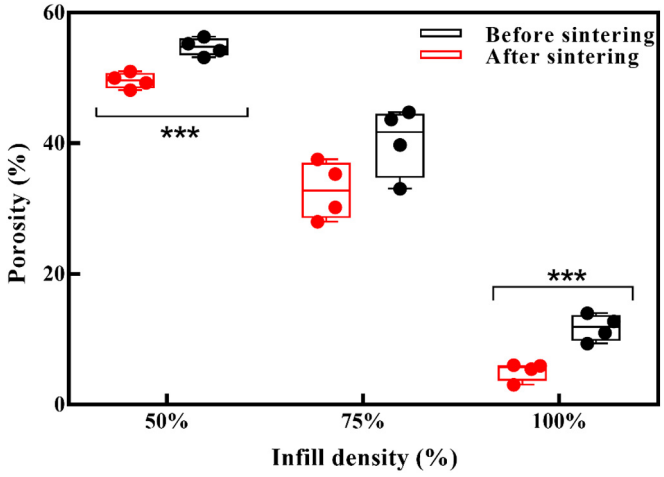

Fig. 4. The percentage porosity obtained from micro-CT analysis of 3D printed HA Cubes at different infill densities before and after sintering to 1350 °C (*** indicates the statistical significance with $P < 0.001$).

Since these scaffolds are intended to be used for load bearing applications, they were tested for their compressive strength as shown in Fig. 5C. Unlike metals and polymers, ceramics hardly exhibit any plastic deformation. As infill density increases in 3D printing ceramic samples, cracks are initiated at different layers and a very irregular stress vs strain pattern can be observed (Fig. 5C). The compressive moduli obtained after mechanical compression testing indicate the increase in mechanical strength as the infill density increases and a maximum Ec (compressive moduli) ~ 275 MPa is found in scaffolds with 100% infill density. The compressive modulus of 50%, 75% and 100% infill samples are around 43 ± 10.78, 184 ± 15.73 and 275 ± 6.27 MPa respectively, which is comparable to the compressive strength of human cortical bone (100 to 150 MPa). Human cortical and trabecular bone are anisotropic in nature; hence their mechanical properties are direction dependent [40]. Mechanical strength of ceramic structures is highly dependent on porosity and direction of loading. As the degree of anisotropy is not significant for all infills in this study (Table 2), the difference in compressive moduli is mainly due to porosity of the scaffolds.

Systematic correlation in mechanical properties with infill density seen here can be exploited to tailor mechanical properties of 3D printed HA based scaffolds. This will help match both mechanical and structural properties of defect with implanted bone graft materials.

Table 2
Table showing the Total porosity (closed + open) percentage before and after sintering, degree of anisotropy (DA) calculated using Micro CT analysis and compressive moduli. *** indicates the ± mean standard deviation.

Sample code	Infill density	% Total porosity		Degree of anisotropy (DA)		Compressive moduli (Ec) in MPa
		Before sintering	After sintering	Before sintering	After sintering	
50% infill	50%	55 ± 1.35	50 ± 1.21	1 ± 0.19	1 ± 0.20	43 ± 10.78
75% infill	75%	40 ± 5.31	33 ± 4.41	1 ± 0.10	1 ± 0.37	184 ± 15.73
100% infill	100%	12 ± 2.04	5 ± 1.40	1 ± 0.10	1 ± 0.13	275 ± 6.27

3.3. 3D printing patient specific defect for radial fracture (case study)

In order to show applicability of 3D printed ceramic (HA) using extrusion based process developed in this study, a case study based on distal radius osteotomy, where a patient specific graft has been designed and printed using patient CT scan has been presented. The aims of case study being evaluating accuracy of scale up of design file and ceramic printing, so that patient specific porous bone graft can be printed which fits within predetermined defect. Fig. 6 shows workflow employed using this study, where 3D reconstruction of bone defect and corresponding bone graft dimension was carried out by clinical team. CAD design was then printed using HA ink formulation developed in this study by scaling up original geometry to 36.86% to account for shrinkage during sintering process as per equation described in Fig. 2. Graft was printed at 60% infill density. The printed graft post sintering and the original design have been compared in terms of geometry. The volume of the designed file to be printed was 1.75 cm^3 and the volume of the 3D printed graft using CT scan volume was found to be 1.83 cm^3, which show the accuracy of ~95.4%. The distance mapping represented in Fig. 6C shows a distance between the printed graft and the defect close to 0.2 mm (blue areas) in most of the graft, with a maximum of 1.5 mm (red areas), suggesting a close matching of the graft inside the corresponding defect. Number of studies have been reported in literature, but they do not focus on reproducibility of the ceramic printing process and limited to standard shapes (cubes). As 3D printing is able to offer complexity of design and manufacturing, complex patient specific defects using pure HA based bio-ink are limited or hardly available to author's knowledge. This study provides a unique insight into reproducibility of extrusion based ceramic printing and its applicability for accurately manufacturing patient specific, porous bone graft materials. There are various applications where a bone graft is required, involving a custom-made graft which can be produced in a simple, reproducible method in a very short time, provides unique opportunity to use this process in dental, orthopaedic and trauma related cases. Pre-design and 3D printed, patient specific graft is likely to reduce operation time, provide enhanced bone healing due to its porous structures and thus help reduce overall direct and indirect cost of surgery. This study also opens further opportunities to use the extrusion based ceramic 3D printing technology for multi-material constructs using different ceramic inks. For example, a porous architecture for trabecular bone regeneration can be incorporated in the internal structure using materials like β-TCP which have high resorption rate and hard external

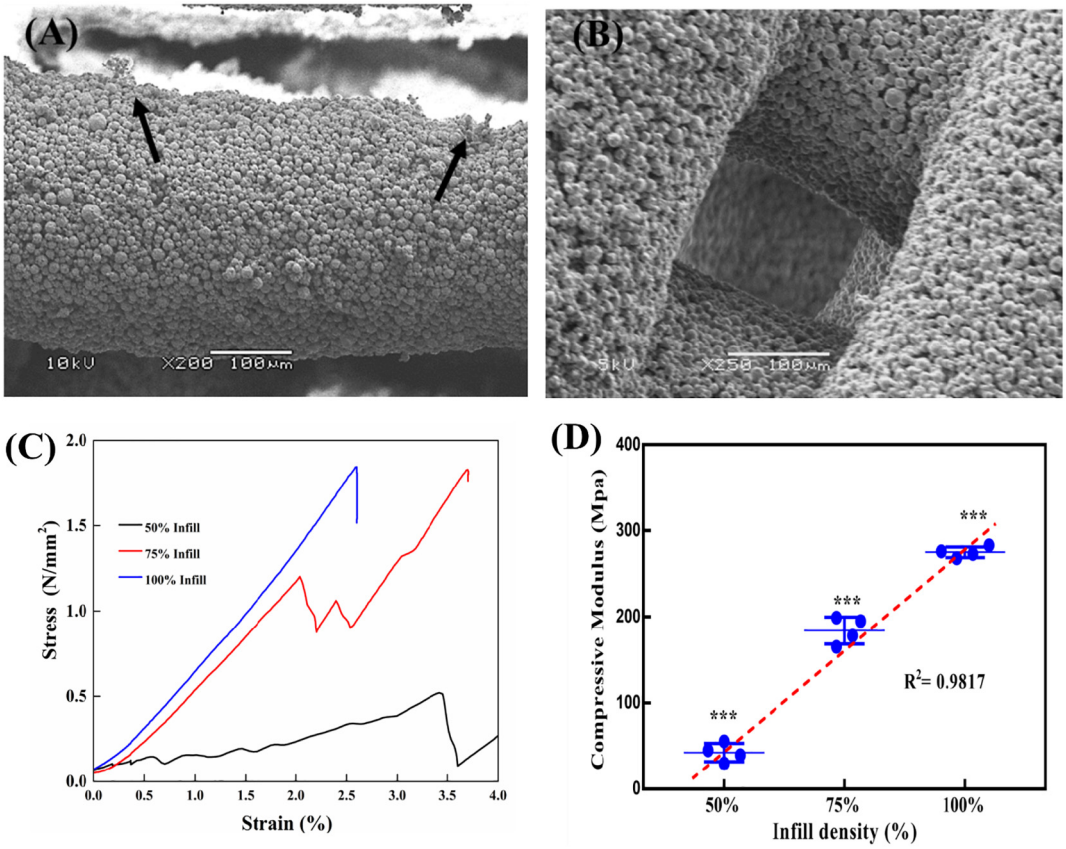

Fig. 5. (A) & (B) are the higher magnification SEM images of 3D printed scaffolds before and after sintering (scale bar 100 μm, black arrows in (A) indicate the presence of polymer binder around particles). (C) is the stress strain cure for different infill densities. (D) is the Scatter plot showing compressive moduli (Ec) of 3D printed HA Cubes at different infill densities heat treated to 1350 °C (*** indicates the statistical significance with $P < 0.001$).

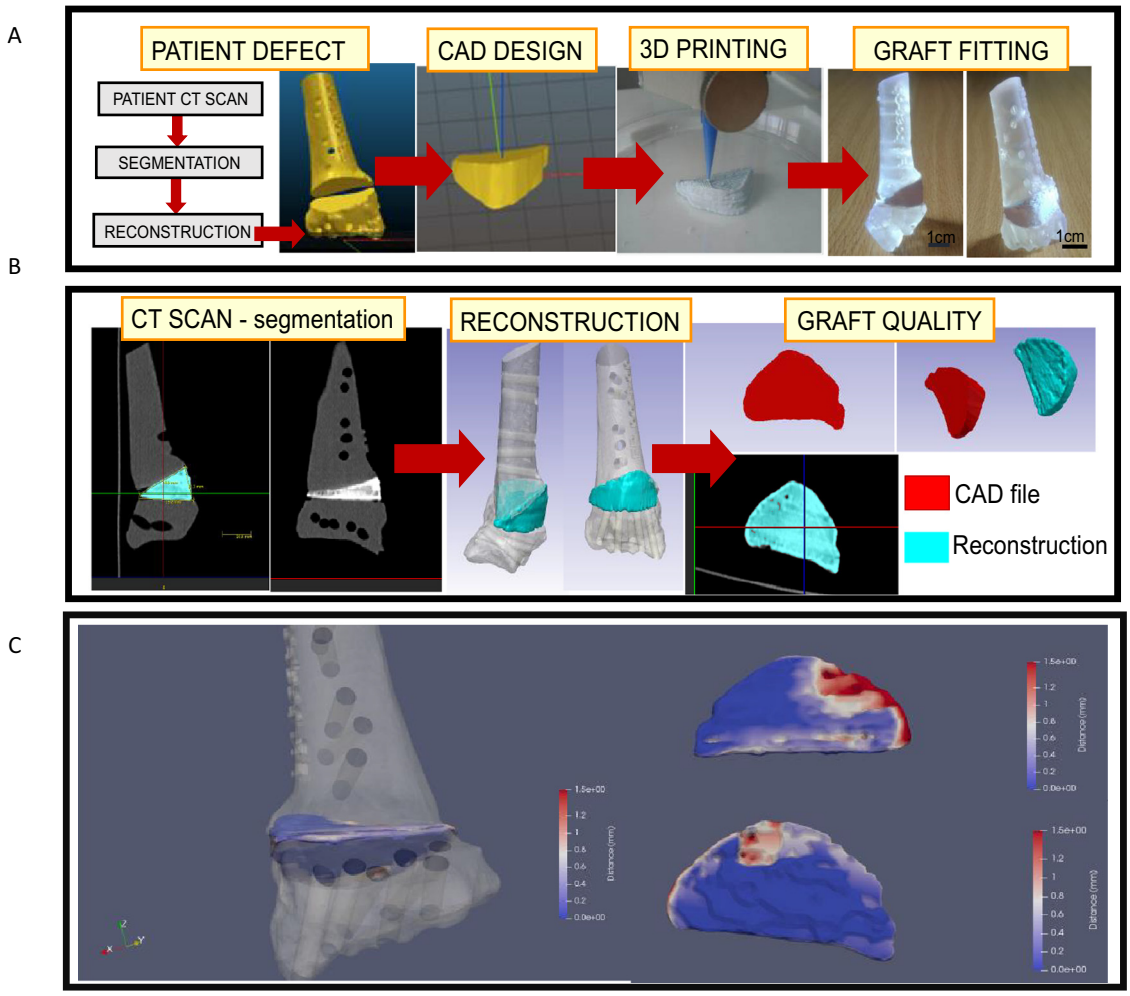

Fig. 6. Validation of the ink formulation and printing process with a clinical case of radial graft osteotomy. A present workflow for converting CT scans to 3D reconstruction of defect and corresponding size of bone graft to be printed. Followed by virtual surgery to fit graft in bone defect. B shows in vitro quality control of graft placement and fit within defect using CT scan. C represents distance map between graft and defect to quantify fitting of 3D printed graft.

architecture can be fabricated using bio-inert materials like zirconia (ZrO_2) which have very high mechanical strength.

4. Conclusion

This study for the first time present the materials and design optimisation for 3D printing of clinically approved hydroxyapatite, so that dimensionally accurate and mechanically stable patient specific complex bony structures can be printed. Materials optimisation was achieved by formulating simple, low cost HA based ink which is capable of printing complex porous shapes.

Understanding relationship between shrinkage of 3D geometry post sintering process of HA based 3D printed structure provides a predictable correlation between design files and final processed objects so that patient specific bone defects can be printed from pre-operative CT scans. This study has implications for materials and 3D design process optimisation for clinical applications. Patient specific bone graft production has potential to reduce need for harvesting autograft and decrease surgery time, whereby impacting overall outcome of the surgery and related costs.

Author contribution

RUK has contributed to optimization of 3D printing of ceramic scaffolds, SEM, mechanical testing, micro CT analysis and written manuscript. SM has carried out 3D printing for clinical case study and reproduced experiments by RUK. AVH has carried out reconstruction of clinical case form CT scans and reviewed manuscript. FV has provided clinical input and validated quality of data and it's relevant for clinical case study. SNR has provided input during data analysis and reviewing manuscript. DMK has led study and supervised work, planned manuscript and reviewed it.

Acknowledgement

The authors wish to acknowledge the financial support provided by Commonwealth scholarship commission under commonwealth split-site scholarship Program, Award reference: INCN-2016-219.

Appendix A. Supplementary data

Supplementary data to this article can be found online at https://doi.org/10.1016/j.matdes.2018.11.054.

References

[1] C. Schopper, F. Ziya-Ghazvini, W. Goriwoda, D. Moser, F. Wanschitz, E. Spassova, G. Lagogiannis, A. Auterith, R. Ewers, HA/TCP compounding of a porous CaP biomaterial improves bone formation and scaffold degradation—a long-term histological study, J Biomed Mater Res B Appl Biomater 74B (1) (2005) 458–467.
[2] S. Bose, D. Banerjee, A. Shivaram, S. Tarafder, A. Bandyopadhyay, Calcium phosphate coated 3D printed porous titanium with nanoscale surface modification for orthopedic and dental applications, Mater. Des. 151 (2018) 102–112.

[3] L.C. Hwa, S. Rajoo, A.M. Noor, N. Ahmad, M.B. Uday, Recent advances in 3D printing of porous ceramics: a review, Curr. Opinion Solid State Mater. Sci. 21 (6) (2017) 323–347.
[4] A. Kumar, S. Mandal, S. Barui, R. Vasireddi, U. Gbureck, M. Gelinsky, B. Basu, Low temperature additive manufacturing of three dimensional scaffolds for bone-tissue engineering applications: processing related challenges and property assessment, Mater. Sci. Eng. R. Rep. 103 (2016) 1–39.
[5] C. Schmidleithner, D. Kalaskar, Stereolithography, 2018.
[6] P. Kunchala, K. Kappagantula, 3D printing high density ceramics using binder jetting with nanoparticle densifiers, Mater. Des. 155 (2018) 443–450.
[7] P. Xuan, M. Liang, Z. Boqing, S. Jianxun, S. Yong, F. Yujiang, G. Zhongru, Z. Changchun, Z. Xingdong, Creating hierarchical porosity hydroxyapatite scaffolds with osteoinduction by three-dimensional printing and microwave sintering, Biofabrication 9 (4) (2017), 045008. .
[8] J.J.A. Barry, A.V. Evseev, M.A. Markov, C.E. Upton, C.A. Scotchford, V.K. Popov, S.M. Howdle, In vitro study of hydroxyapatite-based photocurable polymer composites prepared by laser stereolithography and supercritical fluid extraction, Acta Biomater. 4 (6) (2008) 1603–1610.
[9] O. Guillaume, M.A. Geven, C.M. Sprecher, V.A. Stadelmann, D.W. Grijpma, T.T. Tang, L. Qin, Y. Lai, M. Alini, J.D. de Bruijn, H. Yuan, R.G. Richards, D. Eglin, Surface-enrichment with hydroxyapatite nanoparticles in stereolithography-fabricated composite polymer scaffolds promotes bone repair, Acta Biomater. 54 (2017) 386–398.
[10] K. Takagishi, S. Umezu, Development of the improving process for the 3D printed structure, Sci. Rep. 7 (2017), 39852. .
[11] G.-H. Wu, S.-h. Hsu, Review: polymeric-based 3D printing for tissue engineering, J. Med. Biol. Eng. 35 (3) (2015) 285–292.
[12] G. Varghese, M. Moral, M. Castro-García, J.J. López-López, J.R. Marín-Rueda, V. Yagüe-Alcaraz, L. Hernández-Afonso, J.C. Ruiz-Morales, J. Canales-Vázquez, Fabrication and characterisation of ceramics via low-cost DLP 3D printing, Bol. Soc. Esp. Ceram. Vidrio 57 (1) (2018) 9–18.
[13] S. Buyuksungur, T. Endogan Tanir, A. Buyuksungur, E.I. Bektas, G. Torun Kose, D. Yucel, T. Beyzadeoglu, E. Cetinkaya, C. Yenigun, E. Tonuk, V. Hasirci, N. Hasirci, 3D printed poly(?-caprolactone) scaffolds modified with hydroxyapatite and poly(propylene fumarate) and their effects on the healing of rabbit femur defects, Biomater. Sci. 5 (10) (2017) 2144–2158.
[14] G. Syuhada, G. Ramahdita, A.J. Rahyussalim, Y. Whulanza, Multi-material poly(lactic acid) scaffold fabricated via fused deposition modeling and direct hydroxyapatite injection as spacers in laminoplasty, AIP Conf. Proc. 1933 (1) (2018), 020008. .
[15] L. Simon Joshua, S. Michna, A. Lewis Jennifer, E.D. Rekow, P. Thompson Van, E. Smay James, A. Yampolsky, J.R. Parsons, L. Ricci John, In vivo bone response to 3D periodic hydroxyapatite scaffolds assembled by direct ink writing, J. Biomed. Mater. Res. A 83A (3) (2007) 747–758.
[16] G. Dellinger Jennifer, M. Wojtowicz Abigail, D. Jamison Russell, Effects of degradation and porosity on the load bearing properties of model hydroxyapatite bone scaffolds, J. Biomed. Mater. Res. A 77A (3) (2006) 563–571.
[17] R. Trombetta, J.A. Inzana, E.M. Schwarz, S.L. Kates, H.A. Awad, 3D printing of calcium phosphate ceramics for bone tissue engineering and drug delivery, Ann. Biomed. Eng. 45 (1) (2017) 23–44.
[18] J.A. Inzana, D. Olvera, S.M. Fuller, J.P. Kelly, O.A. Graeve, E.M. Schwarz, S.L. Kates, H.A. Awad, 3D printing of composite calcium phosphate and collagen scaffolds for bone regeneration, Biomaterials 35 (13) (2014) 4026–4034.
[19] R.K. Kankala, K. Zhu, J. Li, C.S. Wang, S.B. Wang, A.Z. Chen, Fabrication of arbitrary 3D components in cardiac surgery: from macro-, micro- to nanoscale, Biofabrication 9 (3) (2017), 032002. .
[20] N. Raja, H.-s. Yun, A simultaneous 3D printing process for the fabrication of bioceramic and cell-laden hydrogel core/shell scaffolds with potential application in bone tissue regeneration, J. Mater. Chem. B 4 (27) (2016) 4707–4716.
[21] D. Hoang, D. Perrault, M. Stevanovic, A. Ghiassi, Surgical applications of three-dimensional printing: a review of the current literature & how to get started, Ann. Transl. Med. 4 (23) (2016) 456.
[22] J. Parthasarathy, 3D modeling, custom implants and its future perspectives in craniofacial surgery, Ann. Maxillofac. Surg. 4 (1) (2014) 9–18.
[23] W. Li, A. Ghazanfari, D. McMillen, M.C. Leu, G.E. Hilmas, J. Watts, Fabricating ceramic components with water dissolvable support structures by the ceramic on-demand extrusion process, CIRP Ann. 66 (1) (2017) 225–228.
[24] M. Faes, H. Valkenaers, F. Vogeler, J. Vleugels, E. Ferraris, Extrusion-based 3D printing of ceramic components, Procedia CIRP 28 (2015) 76–81.
[25] P.H. Warnke, H. Seitz, F. Warnke, S.T. Becker, S. Sivananthan, E. Sherry, Q. Liu, J. Wiltfang, T. Douglas, Ceramic scaffolds produced by computer-assisted 3D printing and sintering: characterization and biocompatibility investigations, J Biomed Mater Res B Appl Biomater 93 (1) (2010) 212–217.
[26] H.N. Chia, B.M. Wu, Recent advances in 3D printing of biomaterials, J. Biol. Eng. 9 (2015).
[27] A. Levy, A. Miriyev, A. Elliott, S.S. Babu, N. Frage, Additive Manufacturing of Complex-shaped Graded TiC/steel Composites, 2017.
[28] J.E.M.T. Jia An, Ratima Suntornnond, Chee Kai Chua, Design and 3D printing of scaffolds and tissues, Engineering 1 (2) (2015) 261–268.
[29] S.V.S. Bose, A. Bandyopadhyay, Bone tissue engineering using 3D printing, Mater. Today 16 (2013).
[30] A. Kumar, A.R. Akkineni, B. Basu, M. Gelinsky, Three-dimensional Plotted Hydroxyapatite Scaffolds With Predefined Architecture: Comparison of Stabilization by Alginate Cross-linking Versus Sintering, 30(8), 2016 1168–1181.
[31] S. Moscato, R. Bahr, T. Le, M. Pasian, M. Bozzi, L. Perregrini, M.M. Tentzeris, Infill-dependent 3-D-printed material based on NinjaFlex filament for antenna applications, IEEE Antennas Wirel. Propag. Lett. 15 (2016) 1506–1509.
[32] A. Sears Nicholas, S. Dhavalikar Prachi, M. Cosgriff-Hernandez Elizabeth, Emulsion inks for 3D printing of high porosity materials, Macromol. Rapid Commun. 37 (16) (2016) 1369–1374.
[33] O. Gauthier, R. Muller, D. von Stechow, B. Lamy, P. Weiss, J.M. Bouler, E. Aguado, G. Daculsi, In vivo bone regeneration with injectable calcium phosphate biomaterial: a three-dimensional micro-computed tomographic, biomechanical and SEM study, Biomaterials 26 (27) (2005) 5444–5453.
[34] H. Seitz, W. Rieder, S. Irsen, B. Leukers, C. Tille, Three-dimensional printing of porous ceramic scaffolds for bone tissue engineering, J Biomed Mater Res B Appl Biomater 74B (2) (2005) 782–788.
[35] A. Niakan, S. Ramesh, P. Ganesan, C.Y. Tan, J. Purbolaksono, H. Chandran, S. Ramesh, W.D. Teng, Sintering behaviour of natural porous hydroxyapatite derived from bovine bone, Ceram. Int. 41 (2, Part B) (2015) 3024–3029.
[36] J. Lefevere, L. Protasova, S. Mullens, V. Meynen, 3D-printing of hierarchical porous ZSM-5: the importance of the binder system, Mater. Des. 134 (2017) 331–341.
[37] C. Bergmann, M. Lindner, W. Zhang, K. Koczur, A. Kirsten, R. Telle, H. Fischer, 3D printing of bone substitute implants using calcium phosphate and bioactive glasses, J. Eur. Ceram. Soc. 30 (12) (2010) 2563–2567.
[38] B.C. Gross, J.L. Erkal, S.Y. Lockwood, C. Chen, D.M. Spence, Evaluation of 3D printing and its potential impact on biotechnology and the chemical sciences, Anal. Chem. 86 (7) (2014) 3240–3253.
[39] T. Ahlfeld, G. Cidonio, D. Kilian, S. Duin, A.R. Akkineni, J.I. Dawson, S. Yang, A. Lode, R.O.C. Oreffo, M. Gelinsky, Development of a clay based bioink for 3D cell printing for skeletal application, Biofabrication 9 (3) (2017), 034103. .
[40] H. Chen, X. Zhou, H. Fujita, M. Onozuka, K.-Y. Kubo, Age-related changes in trabecular and cortical bone microstructure, Int. J. Endocrinol. 2013 (2013) 9.